Magic wavelengths for the $7s_{1/2}$–$6d_{3/2,5/2}$ transitions in Ra^+*

Xiao-Mei Wu(吴晓梅)[1,2], Cheng-Bin Li(李承斌)[1,†], Yong-Bo Tang(唐永波)[3], and Ting-Yun Shi(史庭云)[1]

[1] *State Key Laboratory of Magnetic Resonance and Atomic and Molecular Physics, Wuhan Institute of Physics and Mathematics, Chinese Academy of Sciences, Wuhan* 430071, *China*

[2] *University of Chinese Academy of Sciences, Beijing* 100049, *China*

[3] *Department of Physics, Henan Normal University, Xinxiang* 453007, *China*

(Received 10 April 2016; revised manuscript received 17 May 2016; published online 20 July 2016)

The dynamic polarizabilities of the 7s and 6d states of Ra^+ are calculated using a relativistic core polarization potential method. The magic wavelengths of the $7s_{1/2}$–$6d_{3/2,5/2}$ transitions are identified. Comparing to the common radio-frequency (RF) ion traps, using the laser field at the magic wavelength to trap the ion could suppress the frequency uncertainty caused by the micromotion of the ion, and would not affect the transition frequency measurements. The heating rates of the ion and the powers of the laser for the ion trapping are estimated, which would benefit the possible precision measurements based on all-optical trapped Ra^+.

Keywords: magic wavelength, Dirac–Fock, core polarization

PACS: 31.15.ap, 31.15.bu, 31.30.jc **DOI:** 10.1088/1674-1056/25/9/093101

1. Introduction

The singly charged radium ion Ra^+ has prominent applications in the fields of the precision measurement of time and frequency as well as the test of the fundamental theory of physics.[1–8] Possessing two ultra-narrow forbidden electronic quadrupole transitions $7s_{1/2}$–$6d_{3/2}$ and $7s_{1/2}$–$6d_{5/2}$ in the optical regime, Ra^+ is a promising candidate for the optical atomic clock.[3–5] The precision experiment has been executed for the study of the variation of the fine structure constant α by comparing $^{27}Al^+$ and $^{199}Hg^+$ clocks.[9] Having two optical clock transitions makes Ra^+ a good alternative candidate for testing the variation of α.[5] On the other hand, as the heaviest alkaline earth metal ion, Ra^+ is a good candidate for the study of the atomic parity-nonconservation (PNC). Theoretical works have shown that the 7s $^2S_{1/2}$–6d $^2D_{3/2}$ transition in Ra^+ is sensitive to the PNC effects.[6–8]

To evaluate the accuracies of the potential optical clock, the dipole polarizability is essential for the determination of the energy level shifts due to the stray electromagnetic fields. Theoretically, the determination of the dipole polarizability depends on the electric dipole (E1) matrix elements, while the determination of PNC amplitudes also depends on E1 matrix elements.[1] In the case of Ra^+, E1 matrix elements can be calculated using the modern atomic structure theory methods.[1,7,10] However, there are no experimental reports on the E1 matrix elements of Ra^+.[6]

Nevertheless, the knowledge of the magic wavelengths of the atomic systems could be used to extract out with high precision the transition oscillator strengths,[11] which are connected to the transition matrix elements. The magic wavelength for a transition is the wavelength at which the ac Stark shift of the transition energy is zero.[12] It means that, for the upper and lower energy level of the transition concerned, the difference of the dynamic polarizabilities is zero. The transition frequency measurement at the magic wavelength does not rely on a precision determination of the intensity of the laser field. A notable application of the magic wavelengths is to the optical lattice clocks operated on the neutral atoms.[13] Recent experiments have demonstrated the ability to trap a single ion in the optical lattice.[14,15] Theoretical work pointed out that, compared to the radio-frequency ion traps, the experiments could benefit from the effectively micromotion-free trapping of the ion in an optical trap.[16] It implies that, by choosing a proper laser at the magic wavelength for the clock transition to build the optical trap, it is promising to establish the all-optical trapped ion clocks. Actually, the magic wavelengths for the $4s_{1/2}$–$3d_{5/2}$ transition in Ca^+ have been observed, and meanwhile the ratio of the matrix elements for the $4s_{1/2}$–$4p_{1/2}$ and $4s_{1/2}$–$4p_{3/2}$ has been determined.[17]

For these motivations, we calculated the dynamic polarizabilities of the $7s_{1/2}$, $6d_{3/2}$, and $6d_{5/2}$ states in Ra^+ using the relativistic core polarization potential method. A brief introduction of the computational details will be given in the second section. The magic wavelengths for the $7s_{1/2}$–$6d_{3/2}$ and $7s_{1/2}$–$6d_{5/2}$ transitions are identified. The possibilities of taking advantage of the magic wavelengths to get the transition matrix elements, as well as trapping Ra^+ using the lasers at the wavelengths, are discussed in the third section. Finally, a

*Project supported by the National Basic Research Program of China (Grant No. 2012CB821305) and the National Natural Science Foundation of China (Grant Nos. 91336211 and 11504094).

†Corresponding author. E-mail: cbli@wipm.ac.cn

© 2016 Chinese Physical Society and IOP Publishing Ltd

summary is given in the fourth section. Atomic units are used in this work.

2. Computational details

In the frame of the relativistic core polarization potential method, Ra^+ is simplified as a frozen core part and the valence electron part. The first step is the Dirac–Fock (DF) calculation of the frozen core part based on B-spline basis sets to obtain the core orbital functions, the details of which can be found in our previous work.[11,18] Then a semi-empirical core polarization potential is introduced to approximate the correlation interaction between the core and valence electron and with the functional form

$$V_{\rm pol}(r) = -\sum_{lj} \frac{\alpha_{\rm core}^{(l)} g_{lj}^2(r)}{2r^4} |lj\rangle\langle lj|. \quad (1)$$

Here, $\alpha_{\rm core}^{(l)}$ is the static 2^l-pole polarizability of the core and $g_{lj}^2(r)$ is a cutoff function designed to make the polarization potential finite at the origin, which can be expressed as

$$g_{lj}^2(r) = 1 - \exp\left(-r^6/\rho_{lj}^6\right). \quad (2)$$

The cutoff parameters ρ_{lj} are tuned to reproduce the binding energies of the particular states, to ensure that the calculated energies have at least five significant digits agreed with the data from the NIST database.[19]

In the present work, the basis set of 100 B-splines of $k = 7$ order which are defined on the finite cavity [0, 220 a.u.] is used. A fermi nuclear model is adopted. The potential parameters are shown in Table 1.

Table 1. The core polarizabilities and cut-off parameters for Ra^+ used in the present work.

Parameters	$\alpha_{\rm core}^{(1)}$	$\alpha_{\rm core}^{(2)}$	$\rho_{s_{1/2}}$	$\rho_{p_{1/2}}$	$\rho_{p_{3/2}}$	$\rho_{d_{3/2}}$	$\rho_{s_{5/2}}$
Ra^+	11.66[20]	68.00[20]	2.3162	2.1545	2.2387	2.7703	2.8657

In the calculations, the electron multipole transition operator should include a polarization correction. The modified transition operator is

$$Q_0^{(l)} = r^{(l)} C^{(l)} \left(1 - \frac{\alpha_{\rm core}^{(l)}}{r^{(2l+1)}}(1 - \exp(-r^6/\rho^6))^{1/2}\right). \quad (3)$$

The cutoff parameter ρ used in Eq. (3) is set to $\rho = (\rho_{l_i,j_i} + \rho_{l_f,j_f})/2$, where i and f refer to the initial and final states of the transition. The reduced matrix elements between the low-lying states of Ra^+ obtained by our calculations are shown in Table 2 and compared with the results obtained by the relativistic many-body perturbation theory (RMBPT) method and the relativistic coupled cluster (RCC) method. The differences between our results and other *ab initio* methods are less than 2%.

Table 2. Comparison of the electric dipole reduced matrix elements of Ra^+. RCCSD refers to the RCC method taking into account single and double excitations. RCCSD(T) refers to the RCC method taking into account single, double, and important triple excitations.

Transition	Present	RMBPT[10]	RCCSD[10]	RCCSD(T)[1]
$7s_{1/2}$–$7p_{1/2}$	3.1979	3.1793	3.2545	3.28(2)
$7s_{1/2}$–$7p_{3/2}$	4.4978	3.3881	4.5106	4.54(2)
$6d_{3/2}$–$7p_{1/2}$	3.5570	3.3975	3.5659	3.62(5)
$6d_{3/2}$–$7p_{3/2}$	1.5396	1.4262	1.5117	1.54(2)
$6d_{5/2}$–$7p_{3/2}$	4.8766	4.6240	4.8232	
$6d_{3/2}$–$5f_{5/2}$	4.3908	4.5967	4.4491	
$6d_{5/2}$–$5f_{5/2}$	1.2397	1.3088	1.2465	
$6d_{5/2}$–$5f_{7/2}$	5.5607	5.8347	5.6357	

For an ion in a single-model laser field, the energy shift of a given atomic state i can be written as[21]

$$\Delta E_{\rm i} = -\alpha_i(\omega) I - \gamma_i(\omega) I^2 + O(I^3), \quad (4)$$

where $\alpha_{\rm i}(\omega)$ and $\gamma_{\rm i}(\omega)$ are the dynamic dipole polarizability and hyperpolarizability, respectively. I is the laser intensity and $O(I^3)$ represents the residual high-order Stark shift. The frequency shift of a certain transition caused by the laser field can be written as

$$\begin{aligned} h\Delta\nu &= \Delta E_{\rm f}(\omega) - \Delta E_i(\omega) \\ &= -\Delta\alpha(\omega) I - \Delta\gamma(\omega) I^2 + \Delta O(I^3), \end{aligned} \quad (5)$$

where $\Delta\alpha(\omega)$ and $\Delta\gamma(\omega)$ are the differential dipole polarizability and hyperpolarizability, respectively. Under the weak intensity limit, the frequency shifts contributed by the hyperpolarizability and the residual higher-order terms are several orders of magnitude smaller than the linear term $\Delta\alpha(\omega)I$. So, by ignoring all nonlinear Stark shifts, the magic wavelength can be theoretically given by the condition $\Delta\alpha(\omega) = 0$.[13]

The dynamic dipole polarizability $\alpha_i(\omega)$ can be written as

$$\alpha_i(\omega) = \alpha_i^{\rm S}(\omega) + \frac{3m_i^2 - j_i(j_i+1)}{j_i(2j_i-1)} \alpha_i^{\rm T}(\omega), \quad (6)$$

$$\alpha_i^{\rm S}(\omega) = \frac{2}{(2l+1)(2j_i+1)} \sum_g \frac{\left|\langle\psi_g||D||\psi_i\rangle\right|^2 \varepsilon_{gi}}{\varepsilon_{gi}^2 - \omega^2}, \quad (7)$$

$$\alpha_i^{\rm T}(\omega) = 4\left[\frac{5j_i(2j_i-1)}{6(j_i+1)(2j_i+1)(2j_i+3)}\right] \sum_g (-1)^{j_i+j_g} \times \begin{Bmatrix} j_i & 1 & j_g \\ 1 & j_i & 2 \end{Bmatrix} \frac{\left|\langle\psi_g||D||\psi_i\rangle\right|^2 \varepsilon_{gi}}{\varepsilon_{gi}^2 - \omega^2}, \quad (8)$$

where $\alpha_i^{\rm S}(\omega)$ and $\alpha_i^{\rm T}(\omega)$ are the dynamic scalar and tensor polarizabilities, ω is the photon energy, and $\langle\psi_g||D||\psi_i\rangle$ is the reduced transition matrix element. ε_{gi} is the transition energy and the experimental data from NIST database[19] are used in our calculations. When $\omega = 0$, $\alpha_i^{\rm S}(\omega)$ and $\alpha_i^{\rm T}(\omega)$ refer to the

static scalar and tensor polarizabilities. It should be noted that the tensor component will be taken into account only when $j_i > 1/2$.

3. Results and discussion

3.1. The polarizabilities and the magic wavelengths

The static polarizabilities of the $7s_{1/2}$, $6d_{3/2}$, and $6d_{5/2}$ states in Ra^+ are presented in Table 3. Although the core polarization potential used in this work is semi-empirical, our results are consistent with the results obtained from other *ab initial* methods.[3,4,7]

Table 3. The static scalar and tensor polarizabilities of the $7s_{1/2}$, $6d_{3/2}$, and $5d_{5/2}$ states in Ra^+.

State		Present	Others
$7s_{1/2}$	α^S	103.2131	104.54,[3] 106.12,[4] 106.22[7]
$6d_{3/2}$	α^S	88.6142	83.71,[3] 95.54[4]
	α^T	−49.1487	−50.23[3]
$6d_{5/2}$	α^S	82.1761	82.38[3]
	α^T	−53.2451	−52.60[3]

The dynamic polarizabilities of the $7s_{1/2}$ and $6d_{3/2}$ states are shown in Fig. 1. The photon energies from 0 to 0.15 a.u. are taken into account. Four magic wavelengths of the $7s_{1/2}$–$6d_{3/2}$ transition are identified, two (744.9 nm and 710.3 nm) in the infrared regime and two (435.3 nm and 435.2 nm) in the visible regime. Table 4 shows the contributions of the individual transitions to the polarizabilities of the $7s_{1/2}$ and $6d_{3/2}$ states at the magic wavelengths.

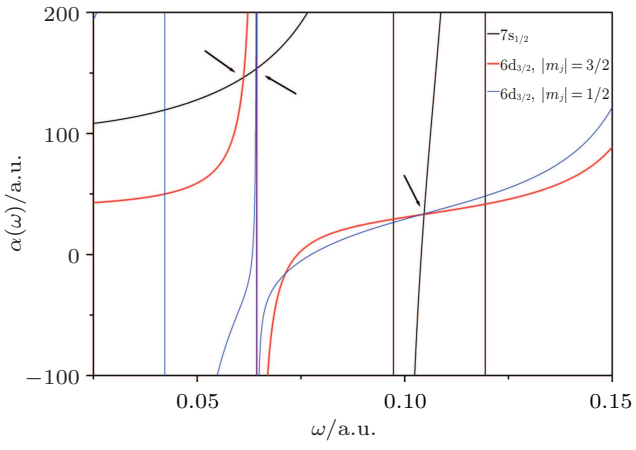


Fig. 1. (color online) The dynamic polarizabilities of the $7s_{1/2}$ and $6d_{3/2}$ states in Ra^+. The magic wavelengths are identified by arrows.

It can be noted from Table 4 that, for the polarizabilities of the $7s_{1/2}$ state at four magic wavelengths, the contributions from $7s_{1/2}$–$7p_{1/2}$ and $7s_{1/2}$–$7p_{3/2}$ transitions are dominant. Meanwhile, for the polarizabilities of the $6d_{3/2,m_j=1/2}$ state at the wavelengths, the contributions from the $6d_{3/2}$–$7p_{1/2}$, $6d_{3/2}$–$7p_{3/2}$, and $6d_{3/2}$–$5f_{5/2}$ transitions are dominant. The contributions from the $6d_{3/2}$–$7p_{3/2}$ and $6d_{3/2}$–$5f_{5/2}$ transitions are dominant for the polarizabilities of the $6d_{3/2,m_j=3/2}$ state at the wavelengths.

Table 4. The contributions of the clock transition $7s_{1/2}$–$6d_{3/2}$ at magic wavelengths within the photon energy range from 0.0 to 0.15 a.u. for Ra^+. The numbers in parentheses are uncertainties in the digits calculated by assuming certain matrix elements have ±2% uncertainties.

ω/a.u.	0.061164(1)	0.064144(1)	0.1046673(8)	0.104676(1)
λ/nm	744.93 (1)	710.3258(1)	435.315(3)	435.277(4)
		$7s_{1/2}$		
$7p_{1/2}$	57.94831	61.99321	−222.39072	−222.10070
$7p_{3/2}$	76.55499	79.37253	243.65931	243.80296
Remainder	0.05639	0.05823	0.09681	0.09682
Core	11.71844	11.72459	11.83870	11.83873
Total	146.27813	153.14856	33.20410	33.63781
		$6d_{3/2}$		
	$m_j = 3/2$	$m_j = 1/2$	$m_j = 3/2$	$m_j = 1/2$
$7p_{1/2}$	0.00000	−76.37284	0.00000	−19.41052
$8p_{1/2}$	0.00000	0.00041	0.00000	0.00056
$7p_{3/2}$	114.24988	187.04887	−6.71716	−0.74614
$5f_{5/2}$	17.61940	26.83761	24.95933	37.44320
$6f_{5/2}$	1.75920	2.66193	2.11420	3.17148
Remainder	0.93121	1.24799	1.00903	1.34050
Core	11.71844	11.72459	11.83870	11.83873
Total	146.27813	153.14856	33.20410	33.63781

Figure 2 shows the dynamic polarizabilities of the $7s_{1/2}$ and $6d_{5/2}$ states. Four magic wavelengths of the $7s_{1/2}$–$6d_{5/2}$ transition are identified, and the contributions of the individual transitions to the polarizabilities of the $7s_{1/2}$ and $6d_{5/2}$ states at these magic wavelengths are tabulated in Table 5. The situation here is similar to that for the $7s_{1/2}$–$6d_{3/2}$ magic wavelengths. The contributions from $7s_{1/2}$–$7p_{1/2}$ and $7s_{1/2}$–$7p_{3/2}$ transitions dominate the polarizabilities of the $7s_{1/2}$ state at four magic wavelengths, while the contributions from the $6d_{5/2}$–$7p_{3/2}$ and $6d_{5/2}$–$5f_{7/2}$ transitions dominate the polarizabilities of the $6d_{5/2}$ state at four magic wavelengths.

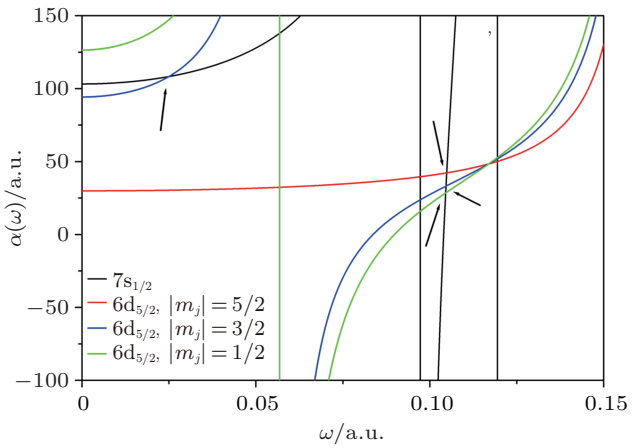


Fig. 2. (color online) The dynamic polarizabilities of the $7s_{1/2}$ and $6d_{5/2}$ states in Ra^+. The magic wavelengths are identified by arrows.

Table 5. The contributions of the clock transition $7s_{1/2}$–$6d_{5/2}$ at magic wavelengths within the photon energy range from 0.0 to 0.15 a.u. for Ra^+. The numbers in parentheses are uncertainties in the digits calculated by assuming certain matrix elements have ±2% uncertainties.

ω/a.u.	0.024974(34)	0.104567(1)	0.104666(1)	0.104863(1)
λ/nm	1824.3894(2.4776)	435.7307(31)	435.3181(32)	434.5007(33)
		$7s_{1/2}$		
$7p_{1/2}$	37.51401	−225.54594	−222.40906	−216.42059
$7p_{3/2}$	59.05428	242.13098	243.65025	246.73031
Remainder	0.04203	0.09668	0.09680	0.09708
Core	11.66738	11.83835	11.83870	11.83939
Total	108.27770	28.52007	33.17669	42.24619
		$6d_{5/2}$		
	$m_j = 3/2$	$m_j = 1/2$	$m_j = 3/2$	$m_j = 5/2$
$7p_{3/2}$	69.20807	−35.04635	−23.30154	−0.00000
$8p_{3/2}$	0.10162	0.23071	0.15396	−0.00000
$5f_{5/2}$	0.84068	0.15825	1.42621	3.97276
$5f_{7/2}$	23.29412	46.82534	39.07418	23.50810
$6f_{7/2}$	2.14348	3.37263	2.81228	1.68947
Remainder	1.02235	1.14114	1.17290	1.23647
Core	11.66738	11.83835	11.83870	11.83939
Total	108.27770	28.52007	33.17669	42.24619

In our previous work on the dynamic polarizabilities of Ca^+,[11] it was suggested that the magic wavelengths of the $4s_{1/2}$–$3d_{5/2}$ transition near 395 nm were measured for the determination of the matrix elements of the 4s–$4p_J$ transitions. This is because the contributions to the polarizabilities from 4s–$4p_J$ transitions are at least two orders of magnitude higher than the contributions from other transitions. But, in the case of Ra^+, the situation is different and more complicated than Ca^+. By measuring two or three magic wavelengths, one might not deduce certain matrix elements with high precision.

3.2. The magic optical trapping of Ra^+

Ra^+ can be laser cooled by taking advantage of the $7s_{1/2}$–$7p_{1/2}$ resonance. The theoretical predicted lifetime of the $7p_{1/2}$ state is 8.72 ns.[7] Then the Doppler cooling limit is about 0.4 mK. With the sideband cooling technology,[22] the temperature of the ion could be of the order of μK. Trapping a single ion Ra^+ by using the laser at the magic wavelengths would benefit the precision measurement on the frequencies of the $7s_{1/2}$–$6d_{3/2}$ and $7s_{1/2}$–$6d_{5/2}$ transitions, since the effectively micromotion-free trapping of the ion in an optical trap would suppress the frequency uncertainty of the measurement, comparing to the common radio frequency Paul traps.[16,23] However, when the ion is trapped in the optical dipole trap, it would be heated by the scattering of the trap photon. The heating rate is associated with the laser intensity and the dynamic polarizability of the quantum state and has the form[24]

$$\gamma_h = \frac{32}{3}\alpha^4\omega^3\,[\alpha(\omega)]^2 I, \tag{9}$$

where α is fine structure constant, ω is the photon energy of the laser field, $\alpha(\omega)$ is the dynamic polarizability, and I is the laser density. For the laser field at the magic wavelength, both the upper and lower states have the same polarizabilities, so they have the same heating rates. The dipole potential can be expressed as[25]

$$U_{\rm dip}(r) = \frac{3\pi c^2}{2\omega_0^3} I(r) \frac{\Gamma_i}{\Delta_i}, \tag{10}$$

where $U_{\rm dip}(r)$ is the dipole potential, $I(r)$ is the field intensity, Γ_i and Δ_i is the natural line-width and the detuning frequency of ith atomic level respectively. Assuming one could build an optical dipole trap with the depth about 4 mK, the related laser intensities and the heating rates are listed in Table 6.

Table 6. The intensity required to build a 4 mK optical dipole trap and the heating rate using the laser at the magic wavelength.

	$7s_{1/2}$–$6d_{3/2}$ transition			
$\lambda_{\rm magic}$/nm	744.93 (1)	710.3258(5)	435.315(3)	435.277(4)
I/kW·cm^{-2}	435	399	88.6	88.7
γ_h/s^{-1}	0.064	0.074	0.003	0.003
	$7s_{1/2}$–$6d_{5/2}$ transition			
$\lambda_{\rm magic}$/nm	1824.3894(2.4776)	435.730(3)	435.318(3)	434.501(3)
I/kW·cm^{-2}	871	87.4	88.6	90.9
γ_h/s^{-1}	0.005	0.002	0.003	0.006

It is noted from Table 6 that both the laser intensities and the heating rates are lower if choosing the lasers at 435 nm. Since 435 nm is near the $7s_{1/2}$–$7p_{1/2}$ resonance, the behavior of dynamic polarizability of the $7s_{1/2}$ state with the variation of the photon energy is steep and $\Delta\alpha(\omega)/\Delta\upsilon$ here is very large. The fluctuation of the laser frequency would cause the heating rate to change dramatically. It is similar for choosing lasers at 744 nm and 710 nm, where $\Delta\alpha(\omega)/\Delta\upsilon$ of the $6d_{3/2}$ state is very large. This is not favorable for the ion trapping. For the laser at 1824 nm, both $\Delta\alpha(\omega)/\Delta\upsilon$ and the heating rate are small. Although 871 kW/cm^2 intensity is required for building a 4 mK optical dipole trap, it is barely achievable by focusing 1 W light with a beam waist diameter of 10 μm. If the high finesse optical cavity could be used, the power of the laser would be lower.

4. Conclusion

The dynamic polarizabilities of the ground state $7s_{1/2}$ and the excited $6d_{3/2,5/2}$ states in Ra^+ are calculated by the relativistic core polarization method, and the magic wavelengths of the $7s_{1/2}$–$6d_{3/2}$ and $7s_{1/2}$–$6d_{5/2}$ transitions are identified. Unlike the case of Ca^+, the contributions to the polarizabilities from individual transitions are more complicated in Ra^+. It might not deduce the transition matrix elements with high precision by the measurements of the magic wavelengths predicted in this work. The heating rates of Ra^+ in the laser field at the magic wavelengths are estimated. The magic wavelength of the $7s_{1/2}$–$6d_{5/2}$ transition near 1824 nm is preferable

for the optical trapping of Ra^+. Optical trapping of the ion is effectively micromotion-free and the precision measurement of the frequency would benefit from it.

Acknowledgment

The authors would like to thank Prof. Guan Hua for the helpful discussion.

References

[1] Sahoo B K, Wansbeek L W, Jungmann K and Timmermans R G E 2009 *Phys. Rev. A* **79** 052512

[2] Versolato O O, Giri G S, Wansbeek L W, van den Berg J E, wan der Hoek D J, Jungmann K, Kruithof W L, Onderwater C J G, Sahoo B K, Santra B, Shidling P D, Timmermans R G E, Willmann L and Wilschut H W 2009 *Phys. Rev. A* **82** 010501

[3] Sahoo B K, Timmermans R G E, Das B P and Mukherjee D 2009 *Phys. Rev. A* **80** 062506

[4] Sahoo B K, Das B P, Chaudhri R K, Mukherjee D, Timmermans R G E and Jungmann K 2007 *Phys. Rev. A* **76** 040504

[5] Versolato O O, Wansbeek L W, Jungmann K, Timmermans R G E, Willmann L and Wilschut H W 2011 *Phys. Rev. A* **83** 043829

[6] Wansbeek L W, Sahoo B K, Timmermans R G E, Jungmann K, Das B P and Mukherjee D 2008 *Phys. Rev. A* **78** 050501

[7] Pal R, Jiang D, Safronova M S and Sfronova U I 2009 *Phys. Rev. A* **79** 062505

[8] Roberts B M, Dzuba V A and Flambaum V V 2014 *Phys. Rev. A* **89** 012502

[9] Rosenband T, Hume D B, Schmidt P O, Chou C W, Brusch A, Lorini L, Oskay W H, Drullinger R E, Fortier T M, Stalnaker J E, Diddams S A, Swann W C, Newbury N R, Itano W M, Wineland D J and Bergquist J C 2008 *Science* **319** 1808

[10] Safronova U I, Johnson W R and Safronova M S 2007 *Phys. Rev. A* **76** 042504

[11] Tang Y B, Qiao H X, Shi T Y and Mitroy J 2013 *Phys. Rev. A* **87** 042517

[12] Katori H, Takamoto M, Pal'chikov V G and Ovsiannikov V D 2003 *Phys. Rev. Lett.* **91** 173005

[13] Derevianko A and Katori H 2011 *Rev. Mod. Phys.* **83** 331

[14] Enderlein M, Huber T, Schneider C and Schartz T 2012 *Phys. Rev. Lett.* **109** 233004

[15] Linnet R B, Leroux I D, Marciante M, Dantan A and Drewsen M 2012 *Phys. Rev. Lett.* **109** 233005

[16] Cormick C, Schaetz T and Morigi G 2011 *New J. Phys.* **13** 043019

[17] Liu P L, Huang Y, Bian W, Shao H, Guan H, Tang Y B, Li C B, Mitroy J and Gao K L 2015 *Phys. Rev. Lett.* **114** 223001

[18] Tang Y B, Li C B and Qiao H X 2014 *Chin. Phys. B* **23** 063101

[19] Kramida A, Ralchenko Y, Reader J and NIST ASD Team 2015 *NIST Atomic Spectra Database* (version 5)

[20] Kaur J, Nandy D K, Arora B and Sahoo B K 2015 *Phys. Rev. A* **91** 012705

[21] Takamoto M, Katori H, Marmo S I, Ovsiannikov V D and Pal'chikov V G 2009 *Phys. Rev. Lett.* **102** 063002

[22] Gong S J, Zhou F, Wu H Y, Wan W, Chen L and Feng M 2015 *Chin. Phys. Lett.* **32** 013201

[23] Schneider C, Enderlein M, Huber T, Dürr S and Schaetz T 2012 *Phys.Rev. A* **85** 013422

[24] Porsev S G, Derevianko A and Fortson E N 2004 *Phys. Rev. A* **69** 021403

[25] Grimm R, Weidemüller M and Ovchinnikov Y B 2000 *Adv. At. Mol. Opt. Phy.* **42** 95